Precise neutron magnetic form factors ☆

G. Kubon [a], H. Anklin [a], P. Bartsch [c], D. Baumann [c], W.U. Boeglin [c,1], K. Bohinc [b],
R. Böhm [c], M.O. Distler [c], I. Ewald [c], J. Friedrich [c], J.M. Friedrich [c], M. Hauger [a],
A. Honegger [a], P. Jennewein [c], J. Jourdan [a,*], M. Kahrau [c], K.W. Krygier [c],
A. Liesenfeld [c], H. Merkel [c], U. Müller [c], R. Neuhausen [c], Ch. Normand [a],
Th. Petitjean [a], Th. Pospischil [c], M. Potokar [b], D. Rohe [a], G. Rosner [c,2], H. Schmieden [c],
I. Sick [a], S. Širca [b], Ph. Trueb [a], A. Wagner [c], Th. Walcher [c], G. Warren [a], M. Weis [c],
H. Wöhrle [a], M. Zeier [a,3], J. Zhao [a], B. Zihlmann [a,4]

[a] *Departament für Physik und Astronomie, Universität Basel, Basel, Switzerland*
[b] *Institute Jožef Stefan, University of Ljubljana, Ljubljana, Slovenia*
[c] *Institut für Kernphysik, Johannes Gutenberg-Universität, Mainz, Germany*

Received 3 August 2001; received in revised form 20 November 2001; accepted 21 November 2001
Editor: J.P. Schiffer

Abstract

Precise data on the neutron magnetic form factor G_{mn} have been obtained with measurements of the ratio of cross sections of $D(e, e'n)$ and $D(e, e'p)$ up to momentum transfers of $Q^2 = 0.9$ (GeV/c)^2. Data with typical uncertainties of 1.5% are presented. These data allow for the first time to extract a precise value of the magnetic radius of the neutron. © 2002 Elsevier Science B.V. All rights reserved.

1. Introduction

Detailed information on the inner structure of the nucleon is provided by accurate data on the dependence of the nucleon form factors on momentum transfer Q^2. Such data serve as a sensitive test for models of the nucleon. Particularly at low Q^2 accurate data on the form factors allow for both a determination of the electromagnetic radii and accurate calculations of nuclear form factors.

While the proton form factors are known with excellent precision over a large range of Q^2, data for the neutron are of much poorer quality due to the lack

of a free neutron target. This is true for both the electric form factor, G_{en}, and to a somewhat lesser extent for the magnetic one, G_{mn}. However, with today's high-duty factor, high-current electron beam facilities and the progress made in polarized beam and target technology, significant progress in this area is being made.

In the past, G_{mn} has been determined mostly from quasi-elastic $D(e, e')$ cross sections (see references in [1]). The extraction of G_{mn} requires a longitudinal/transverse separation and a subtraction of the (dominant) proton magnetic contribution. The uncertainties resulting from the deuteron wave function, meson exchange currents (MEC), and final state interactions (FSI) are greatly amplified by the two subsequent subtractions and limit the accuracy of G_{mn} from these experiments to $\sim$20%. Due to these limitations alternative techniques have been used in recent experiments.

One of the techniques determines G_{mn} from the asymmetry measured in ${}^3\vec{\mathrm{H}}\mathrm{e}(\vec{e}, e')$-scattering [2,3]. This challenging technique is presently limited to low Q^2 where today's rigorous non-relativistic 3-body calculations can be applied to remove the dependence on the nuclear structure, FSI, and MEC [4].

The neutron magnetic form factor can also be obtained from an exclusive cross section measurement of $D(e, e'n)$ [5]. This technique avoids essentially the subtraction of the proton contribution which was responsible for a part of the large sensitivity to systematic errors in the past. However, the method still depends on a deuteron model for the extraction of G_{mn}.

The best method to minimize the sensitivity to the nuclear structure is a determination from the ratio $R = \sigma(e, e'n)/\sigma(e, e'p)$ on the deuteron in quasi-free kinematics [1,6–8]. The ratio is insensitive to the deuteron wave function and corrections due to FSI and MEC are calculable and small. The price to pay is the need for a precise measurement of the *absolute* efficiency η of the neutron detector employed. A measurement of η and a detailed study of the detector response, however, is possible when using high-intensity neutron beams available at the proton-beam facilities [1,7].

In a pilot experiment it was demonstrated that this method leads to a determination of G_{mn} with an accuracy of 1.7% [7]. Similar measurements over

an extended Q^2-region are possible with a high-duty factor electron accelerator like the Mainz Microtron (MAMI) [9]. Precise measurements of the ratio R were performed in the Q^2-range from 0.2 to 0.6 $(\mathrm{GeV}/c)^2$ and values of G_{mn} were extracted with error bars as low as 1% [1]. In the present work we extend the Q^2-range and present data of G_{mn} for Q^2 of 0.071, 0.125, 0.359, 0.894 $(\mathrm{GeV}/c)^2$ in the following labeled as kinematics 1 to 4. To check the consistency of such measurements the point of the pilot experiment [7] has been re-measured (label 2) using a *different* nucleon detector, electron and neutron beam facility.

2. Measurements at MAMI

At MAMI the yield of $D(e, e'n)$ and $D(e, e'p)$ in quasi-elastic kinematics was measured with electron beam energies of 600 MeV and 555 MeV for kinematics 1 and 2 and of 855 MeV for kinematics 3 and 4. A beam current of 0.5 µA incident on a cylindrical 2 cm thick liquid deuterium target cell with 7 µm HAVAR windows was employed for kinematics 2 to 4. Due to the low proton energy (36 MeV) a target cell with a lateral width of only 1 cm liquid deuterium was used for kinematics 1 in order to minimize multiple scattering and energy loss effects of the knocked-out protons. Spectrometer A [10] with a solid angle of 28 msr detected the scattered electron in coincidence with the recoiling nucleon.

The nucleon detector consisted of two 10 cm thick plastic converters, E_f and E_b, preceded by 3 thin ΔE counters used to identify the incident nucleon. The thickness of the ΔE counters was 1.5 mm (5 mm) for kinematics 1 to 2 (3 to 4). Except for the opening towards the target, the detector was shielded with 10 cm thick lead walls. Lead absorbers of 0, 1, 3, and 20 mm thickness were placed at the entrance window of the detector for kinematics 1 to 4. The absorbers are needed in the $D(e, e'n)$ measurements in order to absorb low energy photons. The nucleon detector covered an angular range of $\pm$78 mr in horizontal as well as vertical direction resulting in a solid angle of 24.3 msr.

The yield ratio has been determined via the *simultaneous* measurement of the $D(e, e'n)$ and the $D(e, e'p)$ reactions which makes the ratio independent of the lu-

minosity, dead time effects, and the efficiency of the electron arm. Even at the highest Q^2 a signal-to-noise ratio of $\geqslant 50$ for the $(e, e'n)$ measurement has been achieved.

In the analysis neutrons were defined requiring no hit in at least 2 of the 3 veto counters ($\overline{\Delta E_i}\ \overline{\Delta E_j}$ with $i, j = 1, 2, 3$) and a hit in E_f in the coincident time window. The threshold used in the definition of neutrons in E_f was set at 25 MeV (10 MeV) for kinematics 2 to 4 (1). The number of counted neutrons was corrected for the efficiency of the veto condition and for misidentified protons due to inefficiencies of the veto counters. The veto efficiency correction was determined to $< 1\%$ for kinematics 1 and 2, 11.1% (30.4%) for kinematics 3 (4). The correction for misidentified protons ranged from 0.8% to 5.2%. The three independent measurements for the number of neutrons determined with the three different veto conditions, agreed within 0.16% (1.5%) for kinematics 1 to 3 (4). The agreement of the neutron counts within 1.5% for kinematics 4 provides confidence on the validity of the rather large veto correction.

Protons were counted in the TOF spectrum of E_f with a coincident time signal in one of the three ΔE counters. The number of protons was corrected for the inefficiency of the ΔE counter used. The final number of protons, obtained using different ΔE, E_f combinations, agreed within 0.11% for kinematics 1 to 3 and to 0.2% for kinematics 4. The uncertainty in the corrections to the number of protons and neutrons are small relative to the statistical error and are included in the error of the yield ratios which are summarized in Table 1.

3. Measurements at PSI

The determination of the neutron detection efficiency was performed using the high energy neutron beam (100–590 MeV) at the Paul Scherrer Institut (PSI) [11] for kinematics 2 to 4 and the monoenergetic neutron beam of 68 MeV for kinematics 1 [12].

The high (low) energy neutron beam is produced via the $C(p, n)$ ($D(p, n)$) reaction with a neutron flux of 10^8 s^{-1} (10^6 s^{-1}) for a 5 µA proton beam. A *tagged* high intensity neutron beam was produced via the $H(n, p)n$ reaction, scattering the neutrons from a 1 cm thick liquid H_2-target. The recoil protons

were detected with ΔE_P and E_P plastic scintillators recording the amplitude and the time-of-flight (TOF). Four multi-wire proportional chambers (MWPC) determined the proton trajectory thereby fixing the target coordinates with an accuracy of ± 1.5 mm and the recoil angles with an accuracy of $\pm 0.2°$.

Together with the measured time reference of the radio frequency of the cyclotron, the recorded information allowed for a determination of the incident neutron energy, the energy of the recoiling proton and its recoil angle. This provided a redundant determination of the energy and position of the tagged neutron beam which was free from contributions of background reactions.

The accuracy of the tagged neutron energy from 100 to 490 MeV ranged from 1.9 to 16.6 MeV. For 36 MeV tagged neutrons the energy was determined to an accuracy of 0.2 MeV. The position on the detector surface was determined with an accuracy of ± 3.5 mm.

The nucleon detector was placed in the tagged neutron beam, and its absolute efficiency *distribution* $\eta(x, y, T_n)$ was measured as a function of the point of impact (x, y) and the neutron energy (T_n). The knowledge of the distribution $\eta(x, y, T_n)$ is necessary because the detector illumination is unavoidably different for the $H(n, p)n$ and the $D(e, e'n)$ data taking. Use of the identical configuration during the ratio measurements and the efficiency measurements ensured that absorption effects of neutrons were automatically included in the efficiency determinations. A more detailed account on the neutron efficiency determinations is given in [6,13,14].

Considerable care was taken to ensure identical cuts on the energy deposited in the detectors. $H(e, e'p)$ at MAMI and $H(n, p)$ at PSI were used to obtain absolute calibrations of the amplitude spectrum. In addition, each converter was monitored for both gain variations and baseline shifts using two temperature compensated LED's whose light output was in turn monitored by very stable PIN diodes [7]. This information allowed for a determination of the energy scale of the converters to an accuracy of 0.8% during the PSI and the MAMI runs.

Further corrections, relevant in the determination of R were measured with tagged protons by placing the detector on the recoil arm. The dominant correction of up to $(12.9 \pm 0.7)\%$ was due to multiple scattering and energy loss effects leading to proton losses in

Table 1
Results for R and the experimentally determined errors and corrections in % of R. Except for the yield ratio and η the errors are mainly statistical or systematic in nature

Q^2 (GeV/c)^2	0.071	0.125	0.359	0.894
Yield ratio	±0.5	±1.0	±0.9	±2.1
Illumin. matching	±1.0	±0.5	±0.7	±0.6
Thresh. calibration	±0.8	±0.8	±0.8	±0.8
Proton losses	−7.6 ± 0.9	−11.7 ± 1.0	−8.7 ± 0.7	−12.1 ± 0.7
(p, n)-correction	−0.00 ± 0.02	−0.07 ± 0.02	−0.3 ± 0.1	−1.9 ± 0.6
Error of η	±0.6	±1.0	±0.5	±0.8
T_n and x, y	±0.4	±1.1	±0.6	±0.8
R	0.0973	0.139	0.279	0.311
Rel. error of R in %	±1.7	±2.0	±1.7	±2.7

the lead absorber. In the same arrangement the variation of the light collection efficiency, required to match the measured $\eta(x, y, T_n)$ to the neutron D$(e, e'n)$-distribution, was measured.

Two efficiency measurements bracketed the measurement of the yield ratio at MAMI in order to check the reliability of η. Consistent results for η were found for all kinematic and absorber conditions.

4. Evaluation of R

From the measured yield ratios and efficiencies the D$(e, e'n)$ to D$(e, e'p)$ cross section ratios R^{exp} were determined with accuracies of 1.7% to 2.7%. The resulting values of R^{exp} are independent of the applied E_f threshold. The final results for R^{exp} and the corrections applied in its determination, all of which based on measurements, are summarized in Table 1.

To extract G_{mn} from the measured R^{exp} values we have to take into account the effects of FSI, MEC, and isobar currents (IC) beyond the plane wave impulse approximation (PWIA). To this end, we used theoretical results of R^{theo} calculated with the Paris potential by Arenhövel [15]. The total corrections are listed in Table 2 as a deviation $D = (R_{PWIA}/R^{theo}) - 1$ from the PWIA-value. The dominant contribution to D (up to 99%) is due to FSI, mostly charge exchange scatter-

ing. The contributions from MEC and IC are of order 0.5%, and relativistic effects are negligible [16].

At $Q^2 = 0.071$ (GeV/c)^2 where the correction is largest the dependence of D on the nucleon–nucleon potential was studied. The variation found when using the Bonn R-space, the Argonne V14, and the Paris potential is well within the relative systematic uncertainties (FSI: ±8%, MEC: ±40%, IC: ±60%) used to calculate the errors of Table 2.

The resulting value $R_{PWIA}^{exp} = (\sigma_{e-n}/\sigma_{e-p})_{PWIA} = R^{exp}(1 + D)$ is the experimental ratio of the e–n cross section (which is essentially given by G_{mn}) to the e–p cross section corrected for non-PWIA contributions. The contribution of the neutron electric form factor to R_{PWIA}^{exp} is small; it introduces only a small additional uncertainty despite the poor knowledge of G_{en} (see Table 2).

To evaluate the e–p cross section, σ_{e-p}, we used the world's supply of σ_{e-p} data in a range of 0.5 fm^{-1} around the desired Q. In this range of Q, we used a parameterization with a relative Q-dependence as given by the Mergell et al. fit [17] to G_{ep} and G_{mp}, with the overall normalizations fitted to the world data. The statistical errors of the data have been treated in the standard way, while the systematic errors have been accounted for by changing the data of each set by its error, refitting, and adding the changes due to systematic errors in quadrature. The resulting e–p cross sections relative to the ones obtained with dipole

Table 2
Results for G_{mn} relative to the dipole form factor $G_D = (1 + Q^2/0.710)^{-2}$. The error on G_{mn} includes both the experimental contribution (Table 1, σ_{e-p}, G_{en}) and the ones due to theory

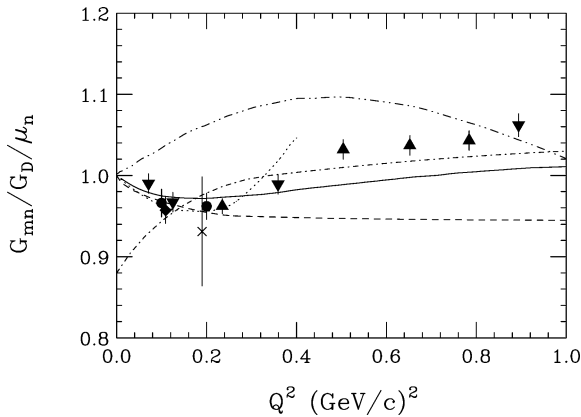| Q^2 (GeV/c)^2	0.071	0.125	0.359	0.894
D (%)	-24.1 ± 2.0	-9.9 ± 0.9	-3.7 ± 0.4	-1.2 ± 0.2
Contr. of G_{en} (%)	-1.4 ± 0.3	-1.9 ± 0.4	-2.8 ± 0.6	-0.6 ± 0.1
σ_{e-p}/σ_D	0.948 ± 0.009	0.931 ± 0.014	0.933 ± 0.019	1.089 ± 0.023
$G_{mn}/(\mu_n G_D)$	0.990 ± 0.013	0.967 ± 0.013	0.989 ± 0.014	1.062 ± 0.017

Fig. 1. The figure shows present results (▼) with the total error bars of Table 2, together with results of the previous MAMI/PSI [1] (▲), the NIKHEF/PSI [7] (♦), the Bates ^{3}He [2] (×), and the JLab ^{3}He experiments [3] (●), in comparison to various model calculations. Solid: Mergell et al. [17], dot: Kubis [18], dash-dot: Eich [19], dash: Schlumpf [20], dash-dot-dot: Lu et al. [21].

form factors are listed in Table 2 together with the final results for G_{mn}.

The present data on G_{mn} are shown in Fig. 1 together with the recently determined data sets (> 1990) of Refs. [1–3,7] and some recent calculations. The present data extend the previously investigated Q^2-region in both directions and allow for a direct comparison of the data measured at NIKHEF/PSI [7] and JLab [3]. The agreement of these data measured with different techniques at different facilities at an unprecedented level of precision is very satisfactory.

On the other hand, these combined data do not agree with the measurements by [5,8] (not shown in Fig. 1). This is due to the fact that in these experiments the three-body reactions D$(e, p)ne'$ and H$(e, \pi)ne'$ were used to tag the recoiling neutron in the η-deter-

mination. This, however, requires significant corrections which were not applied [22].

The data shown in Fig. 1 clearly differ from the crude empirical expression $G_D = (1 + Q^2/m^2)^{-2}$ with $m^2 = 0.71$ (GeV/c)^2 used to remove the dominant Q^2-dependence in Table 2 and Fig. 1. In addition, the data show significant differences to both the non-relativistic constituent quark model calculation by Eich [19], and the relativistic version by Schlumpf [20]. Similar differences are observed when comparing the data to a recent cloudy bag model calculation by Lu et al. [21]. The data are also compared to results of the relativistic chiral perturbation theory by Kubis and Meissner [18] and the calculation by Mergell et al. [17] based on a fit of the proton data using dispersion theoretical arguments. While none of these calculations describe the data satisfactorily the tendency is given by the calculation of Ref. [17].

5. Parameterization of G_{mn}

The present data allow for the first time a purely experimental extraction of the root-mean-square (rms) magnetic radius of the neutron defined as:

$$\langle r_{mn}^2 \rangle = -6 \left(\frac{1}{\mu_n} \frac{dG_{mn}(Q^2)}{dQ^2} \right)_{Q^2=0}. \tag{1}$$

In the past, the experimental information on r_{mn} was based on a dispersion-theoretical analysis of the combined set of electromagnetic form factors of both neutron and proton. In this framework r_{mn} is determined mostly from constraints other than the experimental G_{mn} data which up to now were very limited in accuracy.
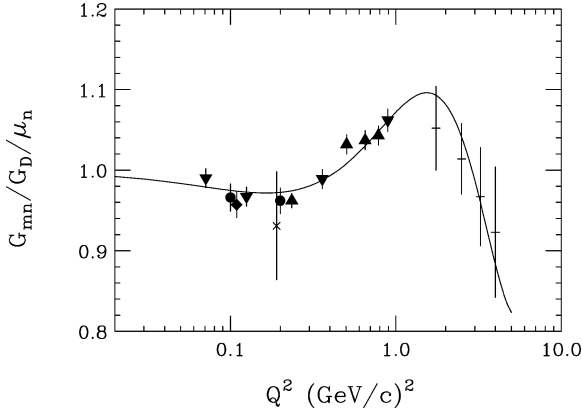
Fig. 2. The figure shows the continued fraction fit to the data. Symbols for the data as in Fig. 1 plus the data by Lung et al. (+) [23].

The present determination of r_{mn} uses *only* the experimental data on G_{mn}. The data of Fig. 1 together with the higher Q^2 data from [23] are taken into account. A continued fraction parameterization given by:

$$G_{mn}(Q^2) = \cfrac{\mu_n}{1 + \cfrac{Q^2 b_1}{1 + \cfrac{Q^2 b_2}{1 + \cdots}}} \qquad (2)$$

is fitted to the data. The magnetic radius of the neutron is related to the parameter b_1 via $\langle r_{mn}^2 \rangle = 6b_1$.

The continued fraction representation [24] has the advantage to converge in a wider domain than the usual power series expansion. One finds, for example, that five terms are sufficient to reproduce G_{mn} of the dispersion analysis by Hoehler [25] or Mergell [17] for Q^2 up to 4 $(\mathrm{GeV}/c)^2$.

Fig. 2 shows the result of the fit using the five terms $b_1, \ldots, b_5 = 3.26$, -0.272, 0.0123, -2.52, 2.55 $(\mathrm{GeV}/c)^{-2}$ with a $\chi_{\mathrm{red}} = 0.91$. For the magnetic radius we find $r_{mn} = 0.873 \pm 0.011$ fm. The uncertainty of 1.1%, an improvement of a factor of 10 compared to previous determinations, covers the error of the fit (0.6%) and a systematic uncertainty due to the choice of the fit function. The latter was determined by fitting pseudo data from a dispersion analysis placed at the Q^2-values and with the errors of the real data.

The present result provides an additional observable to test theoretical calculations of the nucleon. The cal-

culation by Buchmann et al. [26] has been performed in the framework of a constituent quark model including gluon, meson, and confinement exchange currents. The calculation predicts a radius of 0.891 fm in marginal agreement with the present experimental result. The agreement is worse when comparing to the very recent result of 0.84 fm by Kubis and Meissner [18] obtained in fourth order relativistic baryon chiral perturbation theory.

6. Summary

The present data combined with the other data of Fig. 1 have improved our knowledge of the neutron magnetic form factor in the Q^2-range from 0.07 to 0.89 $(\mathrm{GeV}/c)^2$ by a factor of 10 compared to determinations based on quasi-elastic (e, e')-data performed in the past [1]. The improvement is mostly due to the fact that the exploitation of the ratio $R = \sigma(e, e'n)/\sigma(e, e'p)$ depends least on the input of theory; the measurement of R becomes possible by performing the needed calibrations using a high-intensity tagged neutron beam, and by using an electron beam with 100% duty factor. The increase of accuracy allows for a detailed comparison to theoretical model calculations. The agreement of three high-precision experiments gives us confidence in the reliability of the gained knowledge on the magnetic properties of the neutron.

References

[1] H. Anklin et al., Phys. Lett. B 428 (1998) 248.
[2] H. Gao et al., Phys. Rev. C 50 (1994) R546.
[3] W. Xu et al., Phys. Rev. Lett. 85 (2000) 2900.
[4] J. Golak, G. Ziemer, H. Kamada, H. Witala, W. Glöckle, Phys. Rev. C 63 (2001) 034006.
[5] P. Markowitz et al., Phys. Rev. C 48 (1993) R5.
[6] G.P. Kubon, PhD thesis, University of Basel, 1999.
[7] H. Anklin et al., Phys. Lett. B 336 (1994) 313.
[8] E.E.W. Bruins et al., Phys. Rev. Lett. 75 (1995) 21.
[9] H. Herminghaus, H. Euteneuer, K.H. Kaiser, in: Proc. LINAC'90, Albuquerque, NM, USA, 1990, p. 362.
[10] K.I. Blomqvist et al., Nucl. Instrum. Methods A 403 (1998) 263.
[11] J. Arnold et al., Nucl. Instrum. Methods A 386 (1997) 211.
[12] R. Henneck et al., Nucl. Instrum. Methods A 259 (1987) 329.
[13] D. Fritschi, PhD thesis, Basel University, 1993.
[14] P. Trueb, PhD thesis, Basel University, 1995.

[15] W. Fabian, H. Arenhövel, Nucl. Phys. A 314 (1979) 253.

[16] F. Ritz, H. Göller, T. Wilbois, H. Arenhövel, Phys. Rev. C 55 (1997) 2214;
G. Beck, T. Wilbois, H. Arenhövel, Few-body Syst. 15 (1993) 39.

[17] P. Mergell, U.-G. Meissner, D. Drechsel, Nucl. Phys. A 596 (1996) 367.

[18] B. Kubis, U.-G. Meissner, Nucl. Phys. A 679 (2001) 3.

[19] E. Eich, Z. Phys. C 45 (1988) 627.

[20] F. Schlumpf, J. Phys. G 20 (1994) 237.

[21] D.H. Lu, A.W. Thomas, A.G. Williams, Phys. Rev. C 57 (1997) 2628.

[22] J. Jourdan, I. Sick, J. Zhao, Phys. Rev. Lett. 79 (1997) 5186.

[23] A. Lung et al., Phys. Rev. Lett. 70 (1993) 718.

[24] S. Klarsfeld, J. Martorell, J.A. Oteo, M. Nishimura, D.W.L. Sprung, Nucl. Phys. A 456 (1986) 373.

[25] G. Hoehler, E. Pietarinen, I. Sabba-Stefanescu, F. Borkowski, G.G. Simon, V.H. Walther, R.D. Wendling, Nucl. Phys. B 114 (1976) 505.

[26] A. Buchmann, E. Hernandez, K. Yazaki, Nucl. Phys. A 569 (1994) 661.